V/f control for Switched Reluctance Motor

Takahiro Kumagai
Dept. of Science of Technology Innovation
Nagaoka University of Technology
Nagaoka, Japan
kumagai_t1125@ stn.nagaokaut.ac.jp

Jun-ichi Itoh
Dept. of Science of Technology Innovation
Nagaoka University of Technology
Nagaoka, Japan
itoh@vos.nagaokaut.ac.jp

Masakazu Kato
Nagaoka Motor Development Co., Ltd., Japan
kato@nagaoka-md.co.jp

***Abstract*— This paper proposes a novel V/f control method for a switched reluctance motor (SRM). The proposed method does not require the rotor position information and the nonlinear magnetization curve model of SRM. A virtual rotor magnetic flux is generated by controlling the zero-phase current with a PI controller, which realizes the V/f control for SRM. In addition, the maximum torque / current ratio control is achieved by the reactive power in the V/f control. In the proposed simple speed control without a position sensor, the current RMS value is reduced by 43.9% at the torque of 0.1 p.u. compared to without high-efficiency control.**

Keywords—Switched Reluctance Motor, High Efficiency, V/f control, Stabilization Method

I. INTRODUCTION

Recently, high-efficiency motors have been actively studied and developed due to increasing awareness of environmental issues [1-10]. In particular, a switched reluctance motor (SRM) has attracted attention as a variable-speed motor for industrial and home appliance applications such as fans, pumps, and so on, thanks to its rare-earth-element-free, robustness, and cost-effectiveness [4][10]. Therefore, the adjustable speed drive without a position sensor is expected for SRM in order to make use of robustness and cost-effectiveness.

In general, the drive method without the rotor position sensor uses the position dependence of the inductance of SRM [11-13]. In this method, first, the instantaneous value of the inductance is detected from the voltage and the current. Next, the detected inductance is converted to the rotor position information based on the look-up table or the approximation formula of the relationship between the inductance and rotor position. However, complicated control, such as the harmonic voltage superposition or the additional analog circuit, is required to acuuratecy detect the instantaneous value of the inductance [11]. In addition, the nonlinear magnetization curve model of SRM is required for the accurate conversion from the detected inductance into the rotor position, which requires the complicated measurement or finite element analysis (FEA) [12]. Furthermore, the adjustment of the control parameters, such as the current amplitude, turn-on angle, and turn-off angle, is required for the construction of the current and speed controllers with the high torque / current ratio, which requires pre-experiment or FEA [13][14].

This paper proposes a novel V/f control method for SRM drive without the position sensor in order to solve the above problems. The new contribution of the proposed method is the combination of simple speed control and high efficient drive without the position sensor. The V/f control essentially does not require the rotor position information owing to its control strategy based on the rotating coordinate system relative to the inverter output voltage. Therefore, the V/f control does not have the problem of the inductance detection accuracy and the conversion accuracy to the rotor position. Besides, the maximum torque / current ratio control based on the reactive power is applied into the V/f control. This result in both simple speed control and high efficient drive without the rotor position sensor.

Although the principle of the proposed V/f control method for SRM drive is based on the V/f control with the stabilization control and high efficiency control proposed for the PMSM [15]-[18], the following features are mainly different. (A) It is necessary to generate a virtual rotor magnetic flux corresponding to the rotor magnet magnetic flux in PMSM. (B) It is necessary to change the gain of stabilization control since the rotor magnetic flux and inductance dynamically change according to the operating conditions. (C) It is necessary to apply not only i_d=0 but also i_0=i_q for the high efficiency control.

In this paper, first, the proposed method for the above features of (A), (B), and (C) is explained. Next, the usefulness of the proposed V/f control method for SRM drive is confirmed by the experimental results.

II. V/F CONTROL FOR SWITCHED RELUCTANCE MOTOR

Fig.1 shows the control diagram of the proposed V/f control for SRM. The proposed method consists of (A) zero-phase current control, (B) V/f control, and (C) high efficiency control. The details of each control are explained in the following subsections.

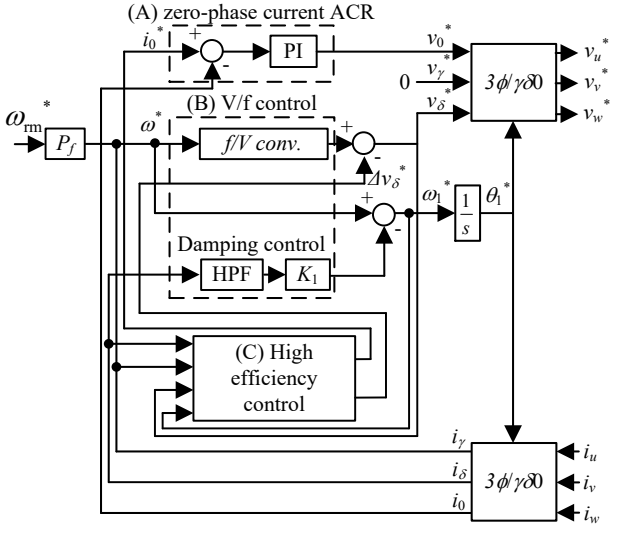

Fig. 1. V/f control method based on γδ axis for SRM.

A. Zero-phase current control

This paper adopts the mathematical model in the Field-Oriented Control (FOC, i.e. vector control) for SRM [19]-[21]. The FOC of SRM uses the dq-axis Cartesian coordinate system with the d-axis defined as the direction of the virtual rotor flux vector generated by the zero-phase current and the q-axis defined as the direction 90 degrees behind the d-axis. In the zero-phase current control, the virtual rotor flux is generated by controlling the zero-phase current with a PI controller, which realizes the V/f control for SRM described in Section B.

B. V/f control

Fig. 2 shows the control block diagram of each servo driver with FOC. PI controller is used for the current control of the d-axis and q-axis. In addition, zero d-axis current control and the feed-forward compensation for canceling the interference of the PM motors are applied.

The proposed control principle is based on the V/f control with the stabilization control [15]-[18], which has been proposed for PMSM. The V/f control uses the γδ-axis Cartesian coordinate system with the γ-axis defined as the direction of the inverter output voltage and the δ-axis defined as the direction 90 degrees behind the γ-axis. In the V/f control for PMSM, the torque oscillation occurs due to the resonance between the moment of inertia and the armature inductance. Then, the torque oscillation is suppressed by the damping control, which feeds back the active current i_δ to the electric angular frequency command ω^* [15]-[18]. In SRM, the same damping control as that for the PMSM is achieved by generating the virtual rotor flux by the zero-phase current control.

Next, the stability and the responsivity of the proposed control are explained. The voltage equation and the torque equation in the γδ-axis Cartesian coordinate system are expressed as in (1) and (2), respectively,

$$\begin{bmatrix} v_\gamma \\ v_\delta \\ v_0 \end{bmatrix} = R\begin{bmatrix} i_\gamma \\ i_\delta \\ i_0 \end{bmatrix} + \begin{bmatrix} L_{dc}+\frac{L_{ac}}{2}\cos(6\theta_1-2\varphi) & -\frac{L_{ac}}{2}\sin(6\theta_1-2\varphi) & \frac{L_{ac}}{\sqrt{2}}\cos(2\varphi) \\ -\frac{L_{ac}}{2}\sin(6\theta_1-2\varphi) & L_{dc}-\frac{L_{ac}}{2}\cos(6\theta_1-2\varphi) & -\frac{L_{ac}}{\sqrt{2}}\sin(2\varphi) \\ \frac{L_{ac}}{\sqrt{2}}\cos(2\varphi) & -\frac{L_{ac}}{\sqrt{2}}\sin(2\varphi) & L_{dc} \end{bmatrix} p\left(\begin{bmatrix} i_\gamma \\ i_\delta \\ i_0 \end{bmatrix}\right)$$
$$+2\omega_1\begin{bmatrix} -L_{ac}\sin(6\theta_1-2\varphi) & -L_{dc}-L_{ac}\cos(6\theta_1-2\varphi) & \frac{L_{ac}}{\sqrt{2}}\sin(2\varphi) \\ L_{dc}-L_{ac}\cos(6\theta_1-2\varphi) & L_{ac}\sin(6\theta_1-2\varphi) & \frac{L_{ac}}{\sqrt{2}}\cos(2\varphi) \\ 0 & 0 & 0 \end{bmatrix}\begin{bmatrix} i_\gamma \\ i_\delta \\ i_0 \end{bmatrix}$$
$$+2p(\delta)\begin{bmatrix} \frac{L_{ac}}{2}\sin(6\theta_1-2\varphi) & \frac{L_{ac}}{2}\cos(6\theta_1-2\varphi) & -\frac{L_{ac}}{\sqrt{2}}\sin(2\varphi) \\ \frac{L_{ac}}{2}\cos(6\theta_1-2\varphi) & -\frac{L_{ac}}{2}\sin(6\theta_1-2\varphi) & -\frac{L_{ac}}{\sqrt{2}}\cos(2\varphi) \\ -\frac{L_{ac}}{\sqrt{2}}\sin(2\varphi) & -\frac{L_{ac}}{\sqrt{2}}\cos(2\varphi) & 0 \end{bmatrix}\begin{bmatrix} i_\gamma \\ i_\delta \\ i_0 \end{bmatrix} \quad (1),$$

$$T = \sqrt{2}PL_{ac}i_0 i_q = \sqrt{2}PL_{ac}i_0(i_\gamma\sin(2\varphi)+i_\delta\cos(2\varphi)) \quad (2),$$

where R is the winding resistance, L_{dc} and L_{ac} are the dc and ac components of the self-inductance, p is the differential operator, ϕ is the deviation angle between γδ-axis Cartesian coordinate and dq-axis Cartesian coordinate, P is the number of pole pairs, and J is the moment of inertia.

The state equation is derived by first ignoring the asynchronous term of (1) appearing as the sixth harmonic for simplification and then performing a linear approximation near the steady-state in the same way as Ref. [15]-[18], and expressed as in (3),

$$p\begin{bmatrix} \Delta i_\gamma \\ \Delta i_\delta \\ \Delta i_0 \\ \Delta\omega \\ \Delta\delta \\ \Delta x \end{bmatrix} = \begin{bmatrix} A_{11} & A_{12} & A_{13} & A_{14} & A_{15} & A_{16} \\ A_{21} & A_{22} & A_{23} & A_{24} & A_{25} & A_{26} \\ A_{31} & A_{32} & A_{33} & A_{34} & A_{35} & A_{36} \\ A_{41} & A_{42} & A_{43} & A_{44} & A_{45} & A_{46} \\ A_{51} & A_{52} & A_{53} & A_{54} & A_{55} & A_{56} \\ A_{61} & A_{62} & A_{63} & A_{64} & A_{65} & A_{66} \end{bmatrix}\begin{bmatrix} \Delta i_\gamma \\ \Delta i_\delta \\ \Delta i_0 \\ \Delta\omega \\ \Delta\delta \\ \Delta x \end{bmatrix} + \begin{bmatrix} B_{11} & B_{12} & B_{13} & B_{14} \\ B_{21} & B_{22} & B_{23} & B_{24} \\ B_{31} & B_{32} & B_{33} & B_{34} \\ B_{41} & B_{42} & B_{43} & B_{44} \\ B_{51} & B_{52} & B_{53} & B_{54} \\ B_{61} & B_{62} & B_{63} & B_{64} \end{bmatrix}\begin{bmatrix} \Delta v_\gamma \\ \Delta v_\delta \\ \Delta v_0 \\ \Delta\omega^* \end{bmatrix} \quad (3),$$

The specific formulas for each element are shown in the appendix.

The following conditions are assumed in order to briefly discuss the stability and response.

(i) No-load condition: $\varphi = 0$, $i_\gamma = 0$, $i_\delta = 0$

(ii) High-speed rotation condition

: w_0L_{dc}, $w_0L_{ac} >> R$, $w_0L_{dc} >> K_1i_\delta$

(iii) The mechanical time constant is sufficiently larger than the electrical time constant: $p(\Delta i_\gamma) = 0$, $p(\Delta i_\delta) = 0$, $p(\Delta i_0) = 0$

(iv) The effect of HPF on stability is small: $p(\Delta x) = 0$

The natural angular frequency ω_n and the damping factor ζ are calculated from the characteristic equation of the second-order system, which is derived by approximating the derived sixth-order state equation expressed as in (1) as a second-order system from the assumption of from (i) to (iv), and expressed as in (4) and (5),

$$\omega_n = \frac{2P\Phi_r}{\sqrt{JL_{dc}}} \quad (4),$$

$$\varsigma = \frac{2}{P}\sqrt{\frac{J}{L_{dc}}}K_1 \quad (5),$$

where

$$\Phi_r = \frac{L_{ac}}{\sqrt{2}}i_0 \quad (6),$$

where K_1 is the damping gain, Φ_r is the virtual rotor flux, and i_0 is the zero-phase current. As shown in Eq.(1), the damping factor ζ is the function of the feedback gain K_1. In other words, the proposed V/f control is stabilized by setting K_1 appropriately. Comparing the natural angular frequency and the damping factor in IPMSM [15]-[18], the rotor magnet magnetic flux corresponds to the virtual rotor magnetic flux. In addition, the q-axis inductance corresponds to the dc components of the self-inductance L_{dc}.

Table 1 shows the motor parameters. The test motor is an 18S/12P type SRM of 750W, 5000r/min (=1 p.u.), and 2.39Nm (=1 p.u.).

Fig.2 shows the loot locus of the sixth-order state equation when damping gain K_1 is increased at no-load and base speed. Note that from No. 1 to No.6 are the characteristic roots of the sixth-order state equation. In this paper, the damping gain K_1 is set so that the real parts of No. 1 and 2 are equal to the real parts of No. 3 and 4 in order to suppress the overshoot of the

TABLE 1 Motor parameters of the test motor

Power	750W
Max. speed (1p.u.)	5000r/min
Max. torque (1p.u.)	2.39Nm
Inverter DC voltage	62V
Poles	18S/12P
Resistance	0.102Ω
AC inductance	0.615mH
DC inductance	1.17mH
Rated current (1 p.u.)	25.4A (i_0, i_q)

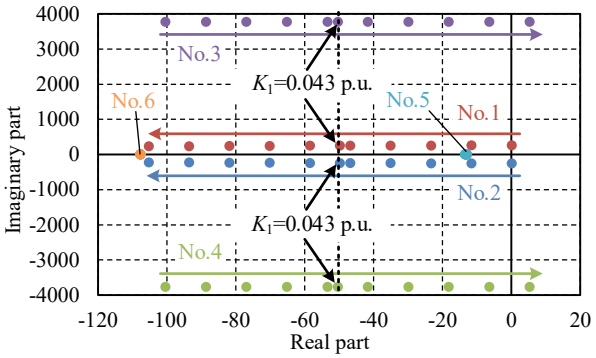

Fig. 2. Loot locus of sixth-order state equation when damping gain K_1 is increased at no-load and base speed.

motor rotation speed [15]-[18]. As shown in Fig. 2, the damping gain K_1 is the optimum value at 0.043 p.u. in this condition. In addition, all roots are located in the left half of the s-plane, i.e., the system is stable.

Fig.3 shows the frequency characteristics of the command speed to the motor speed under no-load and base speed. Note that the figure shows the three conditions of zero-phase current of 0.33 p.u., 0.66 p.u., and 1 p.u. In addition, the damping gain K_1 is set so that the real parts of No. 1 and 2 are equal to the real parts of No. 3 and 4 in each condition. As shown in Fig.3, the calculation results by (3) and the simulation results are almost the same, i.e., the derived sixth-order equation of state-model is valid.

Fig.4 shows the relationship between zero-phase current and natural angular frequency. Note that the calculation results of the natural angular frequency are obtained by using (4). As shown in Fig.4, the calculation results and the simulation results are almost the same, i.e., the characteristic derived by the quadratic system approximation is valid. In this paper, the cutoff frequency of the HPF for stabilization control is set to be 1/20 of the natural frequency ω_n [15]-[18]. In other words, the HPF cutoff frequency ω_c is expressed as in (7).

$$\omega_c = \frac{\omega_n}{20} = \frac{1}{20}\frac{2P\Phi_r}{\sqrt{JL_{dc}}} \qquad (7),$$

Fig.5 shows the relationship between zero-phase current and optimized damping gain K_1. As shown in Fig. 5, the relationship between zero-phase current and optimized damping gain K_1 is inverse proportional. In this proposed method, the damping gain K_1 is applied by varying the gain with respect to the value of the zero-phase current, as shown in Fig.5.

C. *High efficiency control*

Fig.6 shows the control diagram of the high efficiency control for SRM. The torque / current ratio is improved by adjusting the inverter output voltage in the high efficiency

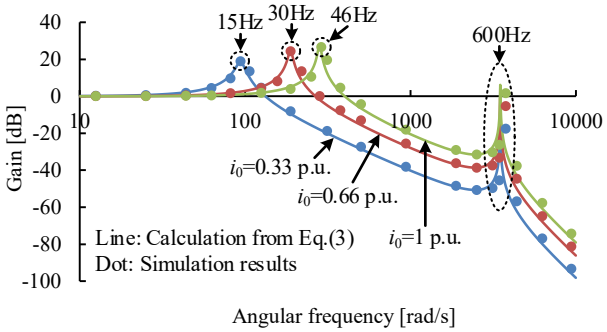

Fig. 3. Frequency characteristics of speed command to motor speed under no-load and base speed (0.6p.u.).

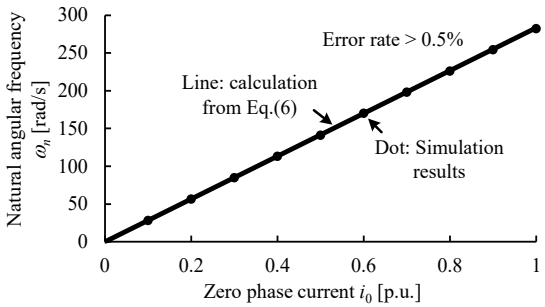

Fig. 4. Relationship between zero-phase current and natural angular frequency

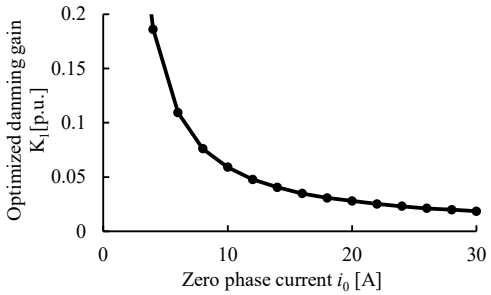

Fig. 5. Relationship between zero phase current and optimized damping gain K_1

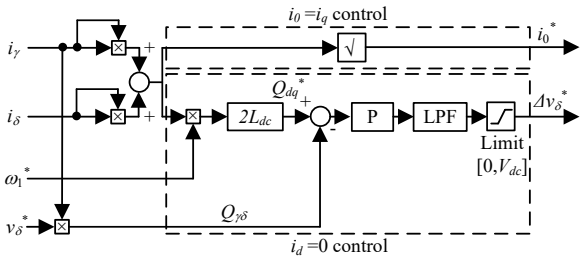

Fig. 6. High efficiency control method

control. The following conditions achieve the maximum torque/current ratio in SRM [19]-[21].

$$i_0 = i_q \qquad (8),$$

$$i_d = 0 \qquad (9),$$

Therefore, it is necessary to apply not only i_d=0 but also i_0=i_q for the high efficiency control.

First, the i_0=i_q control is explained. In the i_d=0 control condition described below, i_q is equal to the AC current amplitude I_{ac}. Therefore, i_0 should be controlled by I_{ac}. In other words, the command value expressed by the following equation should be applied to the command value of zero-phase current control.

$$i_0^* = i_q = I_{ac} = \sqrt{i_\gamma^{\,2} + i_\delta^{\,2}} \quad (10),$$

where i_γ and i_δ are γ-axis and δ-axis current, respectively.

Next, the i_d=0 control is explained. The i_d=0 control is achieved indirectly in the γδ-axis coordinate by focusing on the reactive power of SRM. In the dq-axis coordinate, the reactive power Q_{dq} input into SRM is expressed as in (11).

$$Q_{dq} = v_q i_d - v_d i_q = 2\omega\left\{L_{dc}(i_d^{\,2} + i_q^{\,2}) + L_{ac} i_0 i_d / \sqrt{2}\right\} \quad (11),$$

where v_d and v_q are d-axis and q-axis current respectively. In addition, the reactive power Q_{dq} under the condition of i_d=0 is expressed as in (12),

$$Q_{dq} = 2\omega L_{dc} i_q^{\,2} = 2\omega L_{dc} I_{ac}^{\,2} = 2\omega L_{dc}(i_\gamma^{\,2} + i_\delta^{\,2}) \quad (12),$$

On the other hand, in the γδ-axis coordinate, the reactive power $Q_{\gamma\delta}$ is expressed as in (13),

$$Q_{\gamma\delta} = v_\delta i_\gamma \quad (13),$$

Therefore, the v_δ should be adjusted by the P controller in order to match the reactive power $Q_{\gamma\delta}$ calculated by (4) to the reactive power Q_{dq} calculated by (3). As shown in Fig.2, the value calculated by (2) is applied as the command value for zero-phase current control for the i_0=i_q control. On the other hand, the deviation between (3) and (2) is controlled to be zero by adjusting the v_δ with the P controller for the i_d=0 control. Note that the LPF in the second stage of the P controller shown in Fig.2 is to achieve the i_d=0 control at a steady-state by reducing the gain for high frequencies [15]-[18]. In addition, a limit is provided in order to prevent overcompensation.

III. Experimental Results

Fig. 7 shows the experimental system. The load side servo outputs the arbitrary constant torque. In addition, the instantaneous torque is measured by a high-response torque meter (UTMII-5Nm, 1kHz bandwidth, UNIPULSE). The V/f ratio is set so that the modulation index is 1 at the base speed (0.6 p.u.).

Fig. 8 shows the effect of stabilization control. The speed is 0.6 p.u. and the torque is 0.5 p.u. In the section with the stabilization control, there is no oscillation in the U-phase current and torque. On the other hand, the oscillation occurs and eventually leads to over current after the invalidation of the stabilization control. These results indicate the effectiveness of the stabilization control.

Fig. 9 shows the speed-torque curve. The proposed control achieves the wide range of the drive without the position sensor. Note that the stepping out occurs in the low-speed and large-torque due to the effect of the output voltage error caused by the dead time. In addition, the stepping out also occurs in the high-speed and large-torque. This is because the test SRM is designed for the single-pulse operation at high-speed.

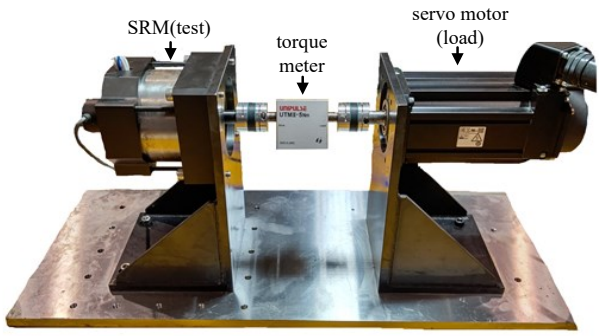

Fig. 7. Experimental equipment.

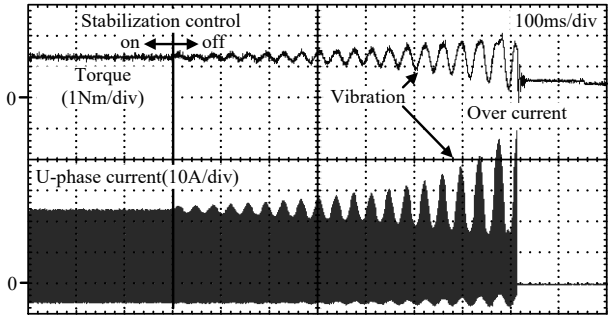

Fig. 8. Effect on the stabilization control.

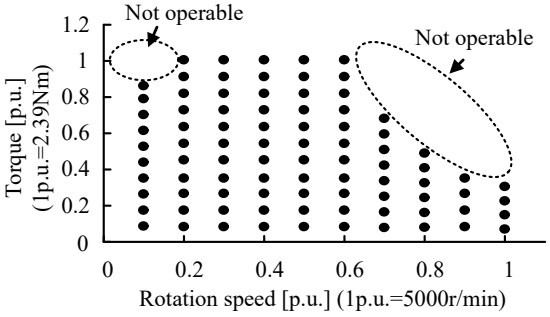

Fig. 9. Speed and torque curves

Fig. 10 shows the effect on the stabilization control with the optimized damping gain. The speed was set to 0.6 p.u. In addition, the torque was set to two conditions of (a) 0.25 p.u. and (b) 1 p.u. The damping gain optimized under the condition of (a) torque 0.25 p.u. is K_1 = 0.059 p.u. On the other hand, The damping gain optimized under the condition of (b) torque 1 p.u. is K_1 = 0.018 p.u. First, the experiments are conducted under inappropriate conditions, and the optimized damping gain K_1 is replaced under both conditions. Next, the optimized appropriate damping gain K_1 is applied under both conditions. As shown in Fig. 11 (a) and Fig. 11 (b), continuous vibration occurs in the torque and current when an inappropriate damping gain K_1 is applied at each operating point. On the other hand, continuous vibration does not occur in the torque and current when an appropriate damping gain K_1 is applied at each operating point. Therefore, the effect on the stabilization control with the optimized damping gain is confirmed.

Fig.11 shows the effect of the high efficiency control at a speed of 0.2 p.u. The current of the the proposed method (V/f control with i_0=i_q and i_d=0) is compared with that FOC with i_0=i_q and i_d=0 and that of V/f control with only i_0=i_q. As a result,

the current RMS value is reduced by 43.9% compared with the only i_0=i_q control at the torque of 0.1 p.u. On the other hand, the current RMS value is increased by 14.8% compared with FOC with the position sensor. However, the increase of the current RMS value becomes small at large torque. Therefore, the proposed drive without the position sensor brings out the same performance as the drive with the position sensor.

IV. Conclusions

This paper proposed a novel V/f control method for SRM. In the control method, a virtual rotor magnetic flux was generated by controlling the zero-phase current with a PI controller, which realized the V/f control for SRM. In addition, the high efficiency control is applied to the V/f control. This result in the achievement of both simple speed control and high efficient drive without the position sensor.

References

[1] M. Okamura, T. Takaoka, "The Evolution of Electric Components in Prius", in *IEEJ Journal of Industry Applications*, Vol. 11, No. 1, pp. 1-6 (2022)

[2] M. Horiuchi, R. Masuda, Y. Bu, M. Nirei, M. Sato, T. Mizuno, "Effect of Magnetic Wedge Characteristics on Torque Ripple and Loss in Interior Permanent Magnet Synchronous Motor", in *IEEJ Journal of Industry Applications*, Vol. 11, No. 1, pp. 49-58 (2022)

[3] K. Takishima, K. Sakai, " Design Method for Ultralightweight Motor Using Magnetic Resonance Coupling and its Characteristics", in *IEEJ Journal of Industry Applications*, Vol. 11, No. 1, pp. 76-87 (2022)

[4] T. Kumagai, H. Sakurai, T. Shioi, H. Kato, J. Itoh, K. Kusaka, T. Yamaguchi, M. Nakagawa, D. Sato, "Experimental Evaluation of Switched Reluctance Motor Made by Blanking Amorphous Alloy Foil", in *IEEJ Journal of Industry Applications*, Vol. 11, No. 1, pp. 117-127 (2022)

[5] Y. Inagaki, M. Mae, O. Shimizu, S. Nagai, H. Fujimoto, T. Miyajima, Y. Yasuda, A. Yamagiwa, "Effect of Harmonic Current Suppression on Iron Loss of IPMSM Using Repetitive Perfect Tracking Control", in *IEEJ Journal of Industry Applications*, Vol. 11, No. 2, pp. 317-326 (2022)

[6] M. Inoue, J. Kitao, Y. Miyama, M. Hazeyama, H. Isoda, H. Arita, K. Nishizawa, T. Nishimura, M. Nakano, "Development of a 48V Integrated Starter Generator for Mild Hybrid Vehicles", in *IEEJ Journal of Industry Applications*, Vol. 11, No. 3, pp. 388-395 (2022)

[7] S. Soma, Y. Kubota, T. Ohzu, "Magnetic Form applying a C-Shaped Magnet for Hybrid Electric Vehicles", in *IEEJ Journal of Industry Applications*, Vol. 11, No. 3, pp. 467-474 (2022)

[8] N. Kawamura, K. Kondo, M. Nagataki, "A Method to Design the Controller for Single Pulse Mode Torque Feedback Control System of IPMSM", in *IEEJ Journal of Industry Applications*, Vol. 11, No. 4, pp. 582-593 (2022)

[9] T. Hirayama, F. Hayashibara, S. Kawabata, "Current Control and Mover Design Method for Thrust Characteristics Improvement of Linear Synchronous Motor with Half-Wave-Rectified Self-Excitation", in *IEEJ Journal of Industry Applications*, Vol. 10, No. 6, pp. 643-651 (2021)

[10] N. Tashiro, K. Nakamura, "A Novel Control Method for In-wheel SR Motor to Implement Torque Vectoring Control for Compact EV", in *IEEJ Journal of Industry Applications*, Vol. 10, No. 6, pp. 708-717 (2021)

[11] K. Ha, R.Y. Kim, and etc.: "Position estimation in switched reluctance motor drive using the first switching harmonics through fourier series", IEEE Trans. on IE, Vol.58, No.12, pp.5352–5360 (2011)

[12] G.G. Lopez, P.C. Kjaer, and T.J.E. Miller: "A new sensorless method for switched reluctance motor drives", IEEE Trans. IA, Vol.34, No.4, pp.832–840 (1998)

[13] I. Husain and S.A. Hossain: "Modeling, Simulation, and Control of Switched Reluctance Motor Drives", IEEE Trans. on IE, Vol.52, No.6, pp.1625–1634 (2005)

[14] K.M. Rahman, B. Fahimi, G. Suresh, A.V. Rajarathnam, and M. Ehsani: "Advantages of Switched Reluctance Motor Applications to EV and HEV: Design and Control Issues", *IEEE Trans. on Ind. Applicat*., Vol.36, No.1, pp.111–121 (2000)

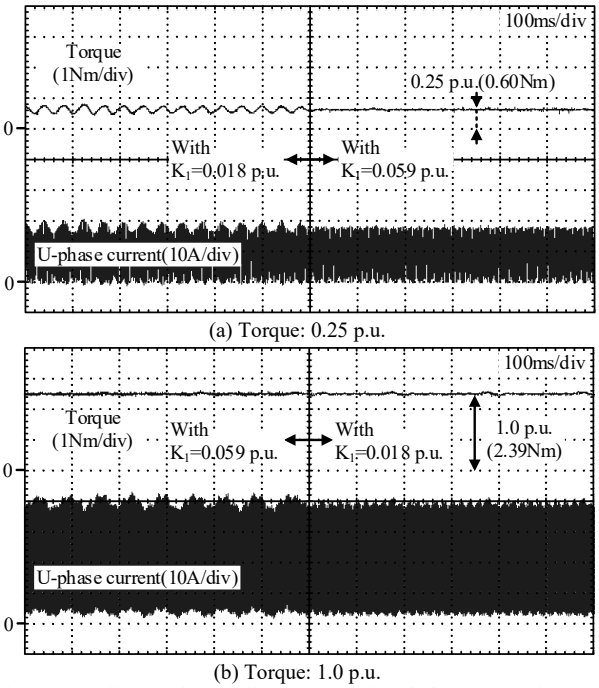

(a) Torque: 0.25 p.u.

(b) Torque: 1.0 p.u.

Fig. 10. Effect on the stabilization control with the optimized damping gain.

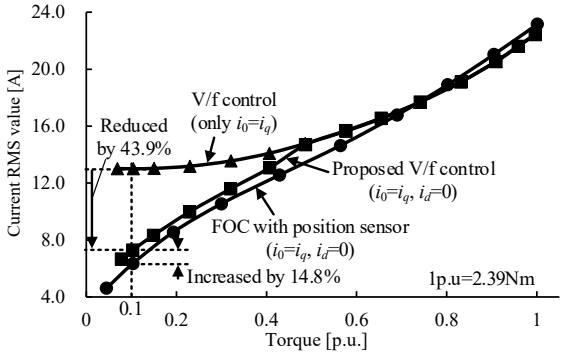

Fig. 11. Effect on the high efficiency control (0.2p.u. speed).

[15] J. Itoh, N. Nomura, and H. Ohsawa, "A comparison between V/f control and position-sensorless vector control for the permanent magnet synchronous motor", PCC2002, pp.1310-1315 (2002)

[16] J. Itoh, T. Toi, M. Kato: "Maximum Torque per Ampere Control Using Hill Climbing Method Without Motor Parameters Based on V/f Control", 18th European Conference on Power Electronics and Applications (EPE'16), Vol. , No. DS3d-Topic 4-0283, (2016)

[17] J. Itoh, T. Toi, K. Nishizawa: "Stabilization Method Using Equivalent Resistance Gain Based on V/f Control for IPMSM with Long Electrical Time Constant", The 2018 International Power Electronics Conference, Vol. , No. 23E1-5, pp. 2229-2236 (2018)

[18] J. Itoh, T. Toi, K. Nishizawa: "Stabilization Method for IPMSM with Long Electrical Time Constant Using Equivalent Resistance Gain Based on V/f Control", IEEJ Transactions on Industry Applications, Vol. 8, No. 4, pp. 592-599 (2019)

[19] N. Nakao and K. Akatsu:"Vector control specialized for switched reluctance motor drives", International Conference on Electrical Machines (ICEM), pp.943-949 (2014)

[20] N. Nakao and K. Akatsu:"Vector control for switched reluctance motor drives using an improved current controller", IEEE Energy Conversion Congress and Exposition (ECCE), pp.1379-1386 (2014)

[21] K.Tokui, T. Kumagai, J. Itoh: "Torque Ripple Suppression Method based on FOC for SRM without FEM Analysis", European Conference on Power Electronics and Applications (EPE) (2021)

APPENDIX

Each element of the state equation (3) are expressed as follows. Note that the subscript "0" indicates the value of the operating point in each variable.

$$A_{11}=\frac{-R\left(L_{dc}{}^2-\frac{L_{ac}{}^2}{2}\sin^2(2\varphi_0)\right)-2\omega_0\left(-\frac{L_{dc}L_{ac}{}^2}{2}\sin(2\varphi_0)\cos(2\varphi_0)\right)}{L_{dc}{}^3-\frac{L_{dc}L_{ac}{}^2}{2}} \tag{A-1}$$

$$A_{12}=\frac{-R\left(-\frac{L_{ac}{}^2}{2}\sin(2\varphi_0)\cos(2\varphi_0)\right)-2\omega_0\left(-L_{dc}{}^3+\frac{L_{dc}L_{ac}{}^2}{2}\sin^2(2\varphi_0)\right)-2K_1(L_{dc}{}^3-\frac{L_{dc}L_{ac}{}^2}{2})i_{\delta 0}}{L_{dc}{}^3-\frac{L_{dc}L_{ac}{}^2}{2}} \tag{A-2}$$

$$A_{13}=\frac{-R\left(-\frac{L_{dc}L_{ac}}{\sqrt{2}}\cos(2\varphi_0)\right)-2\omega_0\frac{1}{\sqrt{2}}\left(L_{dc}{}^2L_{ac}-\frac{L_{ac}{}^3}{2}\right)\sin(2\varphi_0)}{L_{dc}{}^3-\frac{L_{dc}L_{ac}{}^2}{2}} \tag{A-3}$$

$$A_{14}=\frac{-2\left\{\left(-\frac{L_{dc}L_{ac}{}^2}{2}\sin(2\varphi_0)\cos(2\varphi_0)\right)i_{\gamma 0}+\left(-\frac{L_{dc}L_{ac}{}^2}{2}\cos^2(2\varphi_0)\right)i_{\delta 0}+\frac{1}{\sqrt{2}}\left(L_{dc}{}^2L_{ac}-\frac{L_{ac}{}^3}{2}\right)\sin(2\varphi_0)i_{00}\right\}}{L_{dc}{}^3-\frac{L_{dc}L_{ac}{}^2}{2}} \tag{A-4}$$

$$A_{15}=\frac{-4\omega_0\left\{\frac{L_{dc}{}^2L_{ac}}{\sqrt{2}}\cos(2\varphi_0)i_{00}\right\}}{L_{dc}{}^3-\frac{L_{dc}L_{ac}{}^2}{2}} \tag{A-5}$$

$$A_{16}=2K_1i_{\delta 0} \tag{A-6}$$

$$A_{21}=\frac{-R\left(-\frac{L_{ac}{}^2}{2}\sin(2\varphi_0)\cos(2\varphi_0)\right)-2\omega_0\left(L_{dc}{}^3-\frac{L_{dc}L_{ac}{}^2}{2}\cos^2(2\varphi_0)\right)}{L_{dc}{}^3-\frac{L_{dc}L_{ac}{}^2}{2}} \tag{A-7}$$

$$A_{22}=\frac{-R\left(L_{dc}{}^2-\frac{L_{ac}{}^2}{2}\cos^2(2\varphi_0)\right)-2\omega_0\left(\frac{L_{dc}L_{ac}{}^2}{2}\sin(2\varphi_0)\cos(2\varphi_0)\right)+2K_1(L_{dc}{}^3-\frac{L_{dc}L_{ac}{}^2}{2})i_{\gamma 0}}{L_{dc}{}^3-\frac{L_{dc}L_{ac}{}^2}{2}} \tag{A-8}$$

$$A_{23}=\frac{-R\left(\frac{L_{dc}L_{ac}}{\sqrt{2}}\sin(2\varphi_0)\right)-2\omega_0\frac{1}{\sqrt{2}}\left(L_{dc}{}^2L_{ac}-\frac{L_{ac}{}^3}{2}\right)\cos(2\varphi_0)}{L_{dc}{}^3-\frac{L_{dc}L_{ac}{}^2}{2}} \tag{A-9}$$

$$A_{24}=\frac{-2\left\{\left(\frac{L_{dc}L_{ac}{}^2}{2}\sin^2(2\varphi_0)\right)i_{\gamma 0}+\left(\frac{L_{dc}L_{ac}{}^2}{2}\sin(2\varphi_0)\cos(2\varphi_0)\right)i_{\delta 0}+\frac{1}{\sqrt{2}}\left(L_{dc}{}^2L_{ac}-\frac{L_{ac}{}^3}{2}\right)\cos(2\varphi_0)i_{00}\right\}}{L_{dc}{}^3-\frac{L_{dc}L_{ac}{}^2}{2}} \tag{A-10}$$

$$A_{25}=\frac{-4\omega_0\left\{-\frac{L_{dc}{}^2L_{ac}}{\sqrt{2}}\sin(2\varphi_0)i_{00}\right\}}{L_{dc}{}^3-\frac{L_{dc}L_{ac}{}^2}{2}} \tag{A-11}$$

$$A_{26}=-2K_1i_{\gamma 0} \tag{A-12}$$

$$A_{31}=\frac{-R\left(-\frac{L_{dc}L_{ac}}{\sqrt{2}}\cos(2\varphi_0)\right)-2\omega_0\left(\frac{L_{dc}{}^2L_{ac}}{\sqrt{2}}\sin(2\varphi_0)\right)}{L_{dc}{}^3-\frac{L_{dc}L_{ac}{}^2}{2}} \tag{A-13}$$

$$A_{32}=\frac{-R\left(\frac{L_{dc}L_{ac}}{\sqrt{2}}\sin(2\varphi_0)\right)-2\omega_0\left(\frac{L_{dc}{}^2L_{ac}}{\sqrt{2}}\cos(2\varphi_0)\right)}{L_{dc}{}^3-\frac{L_{dc}L_{ac}{}^2}{2}} \tag{A-14}$$

$$A_{33}=\frac{-RL_{dc}{}^2}{L_{dc}{}^3-\frac{L_{dc}L_{ac}{}^2}{2}} \tag{A-15}$$

$$A_{34}=\frac{-2\left\{\left(\frac{L_{dc}{}^2L_{ac}}{\sqrt{2}}\sin(2\varphi_0)\right)i_{\gamma 0}+\left(\frac{L_{dc}{}^2L_{ac}}{\sqrt{2}}\cos(2\varphi_0)\right)i_{\delta 0}\right\}}{L_{dc}{}^3-\frac{L_{dc}L_{ac}{}^2}{2}} \tag{A-16}$$

$$A_{35}=\frac{-4\omega_0\left\{-\frac{L_{dc}L_{ac}{}^2}{2}i_{00}\right\}}{L_{dc}{}^3-\frac{L_{dc}L_{ac}{}^2}{2}} \tag{A-17}$$

$$A_{41}=\frac{\sqrt{2}P^2L_{ac}}{J}i_{00}\sin(2\varphi_0) \tag{A-18}$$

$$A_{42}=\frac{\sqrt{2}P^2L_{ac}}{J}i_{00}\cos(2\varphi_0) \tag{A-19}$$

$$A_{43}=\frac{\sqrt{2}P^2L_{ac}}{J}\left(i_{\gamma 0}\sin(2\varphi_0)+i_{\delta 0}\cos(2\varphi_0)\right) \tag{A-20}$$

$$A_{45}=\frac{\sqrt{2}P^2L_{ac}}{J}\left(2i_{\gamma 0}i_{00}\cos(2\varphi_0)-2i_{\delta 0}i_{00}\sin(2\varphi_0)\right) \tag{A-21}$$

$$A_{52}=-K_1 \tag{A-22}$$

$$A_{54}=-1 \tag{A-23}$$

$$A_{56}=K \tag{A-24}$$

$$A_{62}=\frac{1}{\tau} \tag{A-25}$$

$$A_{66}=-\frac{1}{\tau} \tag{A-26}$$

$$A_{otherwise}=0 \tag{A-27}$$

$$B_{11}=\frac{L_{dc}{}^2-\frac{L_{ac}{}^2}{2}\sin^2(2\varphi_0)}{L_{dc}{}^3-\frac{L_{dc}L_{ac}{}^2}{2}} \tag{A-28}$$

$$B_{12}=\frac{-\frac{L_{ac}{}^2}{2}\sin(2\varphi_0)\cos(2\varphi_0)}{L_{dc}{}^3-\frac{L_{dc}L_{ac}{}^2}{2}} \tag{A-29}$$

$$B_{13}=\frac{-\frac{L_{dc}L_{ac}}{\sqrt{2}}\cos(2\varphi_0)}{L_{dc}{}^3-\frac{L_{dc}L_{ac}{}^2}{2}} \tag{A-30}$$

$$B_{21}=\frac{-\frac{L_{ac}{}^2}{2}\sin(2\varphi_0)\cos(2\varphi_0)}{L_{dc}{}^3-\frac{L_{dc}L_{ac}{}^2}{2}} \tag{A-31}$$

$$B_{22}=\frac{L_{dc}{}^2-\frac{L_{ac}{}^2}{2}\cos^2(2\varphi_0)}{L_{dc}{}^3-\frac{L_{dc}L_{ac}{}^2}{2}} \tag{A-32}$$

$$B_{23}=\frac{\frac{L_{dc}L_{ac}}{\sqrt{2}}\sin(2\varphi_0)}{L_{dc}{}^3-\frac{L_{dc}L_{ac}{}^2}{2}} \tag{A-33}$$

$$B_{31}=\frac{-\frac{L_{dc}L_{ac}}{\sqrt{2}}\cos(2\varphi_0)}{L_{dc}{}^3-\frac{L_{dc}L_{ac}{}^2}{2}} \tag{A-34}$$

$$B_{32}=\frac{\frac{L_{dc}L_{ac}}{\sqrt{2}}\sin(2\varphi_0)}{L_{dc}{}^3-\frac{L_{dc}L_{ac}{}^2}{2}} \tag{A-35}$$

$$B_{33}=\frac{L_{dc}{}^2}{L_{dc}{}^3-\frac{L_{dc}L_{ac}{}^2}{2}} \tag{A-36}$$

$$B_{14}=2i_{\delta 0} \tag{A-37}$$

$$B_{24}=-2i_{\gamma 0} \tag{A-38}$$

$$B_{54}=1 \tag{A-39}$$

$$B_{otherwise}=0 \tag{A-40}$$